

Design of Moiré-Inspired Metasurface Lens for Focusing Electromagnetic Power in Fresnel Near-Field Region

Tae-Heung Lim ¹, Hyunsoo Kim ², Chulhun Seo ³ and Hosung Choo ^{4,*} 

¹ Department of Electrical Engineering, Ulsan National Institute of Science and Technology (UNIST), Ulsan 44919, Korea; limth0105@unist.ac.kr

² Electronic Warfare R&D, LIG Nex1 Co., Sungnam 13488, Korea; hyunsoo.kim@lignex1.com

³ School of Electronic Engineering, Soongsil University, Seoul 06978, Korea; chulhun@ssu.ac.kr

⁴ School of Electronic and Electrical Engineering, Hongik University, Seoul 04066, Korea

* Correspondence: hschoo@hongik.ac.kr

Abstract: This paper proposes a Moiré-inspired metasurface lens system to focus electromagnetic power in the Fresnel near-field region. The proposed metasurface lens (MSL) system is composed of two MSLs and a square patch antenna source. The MSLs are modeled based on the transmit phase distributions of Moiré lens theory, and each unit cell structure (patch shape and Jerusalem cross slot shape) is determined to fit the calculated transmit phase distributions at each location. When changing the unit cell structure, phase and transmittance variations are achieved over 330° and −3 dB. The square patch antenna source is then designed to excite the field to the MSLs. The measured reflection coefficients are below −10 dB at 5.8 GHz while rotating the second MSL. The focal length can be adjusted from a minimum of 38 cm to a maximum of 110 cm according to the rotation angle of the second MSL. The proposed MSL system can be employed for wireless power transmission applications to focus electromagnetic power at various locations in the near-field region.



Citation: Lim, T.-H.; Kim, H.; Seo, C.; Choo, H. Design of Moiré-Inspired Metasurface Lens for Focusing Electromagnetic Power in Fresnel Near-Field Region. *Energies* **2022**, *15*, 3911. <https://doi.org/10.3390/en15113911>

Academic Editors: Mauro Feliziani and Andrea Mariscotti

Received: 6 April 2022

Accepted: 24 May 2022

Published: 25 May 2022

Publisher's Note: MDPI stays neutral with regard to jurisdictional claims in published maps and institutional affiliations.



Copyright: © 2022 by the authors. Licensee MDPI, Basel, Switzerland. This article is an open access article distributed under the terms and conditions of the Creative Commons Attribution (CC BY) license (<https://creativecommons.org/licenses/by/4.0/>).

Keywords: Moiré lens; focusing electromagnetic power; Fresnel near-field beam focusing; metasurface; wireless power transmission

1. Introduction

Over the past decade, beam-focusing technologies in the Fresnel near-field region have been dramatically developed for various applications such as biosensing, radio wave therapy, wireless power transmission (WPT), and RFID [1–5]. In general, to focus the electromagnetic power of the beam in the near-field region, a WPT system is designed by using numerous array antenna elements or a large aperture antenna. In addition, such antennas require phase shifters, and power amplifiers for each element to adjust the beam direction and focal point. A number of studies have investigated near-field beam focusing by adjusting phase and amplitude excitation for each array element. For example, feeding networks using microstrip lines, coplanar wave guides, and substrate integrated waveguides are designed to implement the microstrip patch array antenna based on optimal phase and amplitude distributions [6–8]. Other studies employing digital or analog phase shifters for each array element to adjust the near-field beam have also been introduced [9–13]. Although these techniques can provide high-performance of near-field beam focusing in WPT applications, the antenna system has disadvantages of a complicated feeding network and an expansive fabrication cost for the phase shifters. To overcome these problems, meta-inspired transmission surfaces and dielectric lenses are often used to steer the radiation beam and to obtain high-directive radiation patterns at a low cost with a simple fabrication [14–17]. However, such designs for the beam adjustments are mainly considered on the radiation beam in the far-field region.

In this paper, we propose a Moiré-inspired metasurface lens for adjusting the focal point of the electromagnetic power in the Fresnel near-field region. The proposed meta-

surface lens (MSL) system is composed of two lenses and a square patch antenna source. Transmitting phase distributions for the two MSLs are calculated using Moiré lens theory, and each unit cell shape is decided to fit transmit phase distributions at each location. The unit cell structure consists of two square patches and one Jerusalem cross slot patch printed on three dielectric layers with air gaps. By changing the unit cell structure, phase variation and transmittance can be achieved over 330° and -3 dB. The square patch antenna source printed on a single dielectric substrate is then designed to excite the field to the MSLs. The proposed MSL system is modeled using the FEKO full electromagnetic (EM) simulation software tool [18] to observe transmitting phase distributions and near-field beam for focusing the electromagnetic power. To confirm its feasibility, the MSL system is fabricated, and its near-field and impedance matching characteristics are measured to observe the adjustment of near-field beam focusing according to the MSL rotation angle. We additionally observe the transmission efficiency of the MSLs and the wireless power transfer efficiency at the focal length in accordance with the rotation angle for employing the practical wireless power transfer applications. The results confirm that the proposed MSLs are capable of achieving electromagnetic power focusing at various distances in the Fresnel near-field region with a simple and low-cost fabrication.

2. Moiré-Inspired MSL System

2.1. Theoretical Background: Moiré Lens

Figure 1 shows the geometry of the proposed Moiré-inspired MSL system for focusing electromagnetic power in the Fresnel near-field region. The proposed MSL system consists of a patch antenna source and two MSLs: Lens 1 (T_1) and Lens 2 (T_2), where each lens is designed to have the same radius R . The square patch antenna is used as a source to excite the MSLs, and the near-field beam is concentrated on the green point (A). When T_2 is rotated by an angle θ_r , the focal point is adjusted to the blue point (B) by changing the electromagnetic power concentration of the beam in the near-field region. This beam focusing technique is commonly employed in optics for the Moiré lens [19–21].

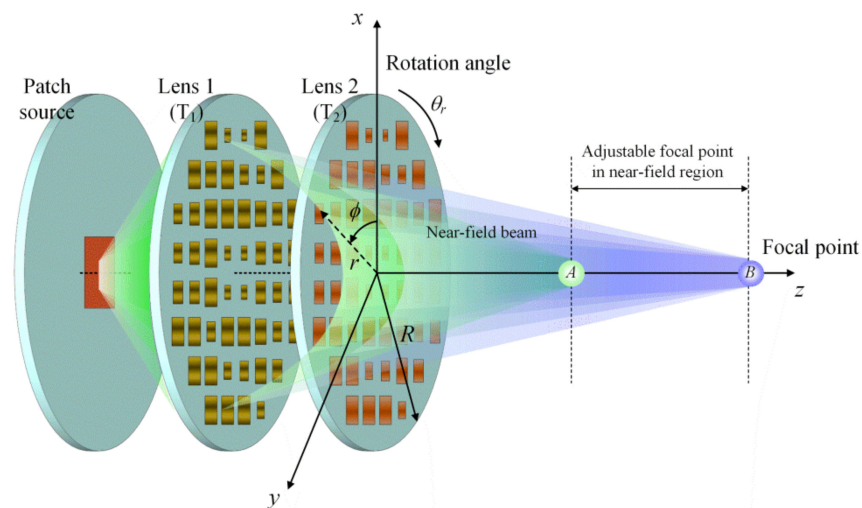


Figure 1. Geometry of the proposed Moiré-inspired MSL system for focusing electromagnetic power in the Fresnel near-field region.

The theoretical background relates to the Moiré lens, in which various beam can be generated when two different lenses having periodic structures are superimposed [22–24]. Figure 2a,b illustrate the transmitting phase distributions of T_1 and T_2 , respectively, based on the Moiré lens theory. T_1 and T_2 are complex conjugates of each other, and the resulting phase distributions can be calculated using the equations as follows [19]:

$$T_1 = \arg \left[\exp \left\{ jk \left(ar^2 \right) \phi \right\} \right], \quad (1)$$

$$T_2 = T_1^* = \arg \left[\exp(-jk(ar^2)\phi) \right], \quad (2)$$

where r is the distance from the lens center to each cell location; ϕ is the angle from the x -axis to each unit cell; a is an amplifying constant for the parabolic Fresnel lens equation of ar^2 [19]; and k is a wave number.

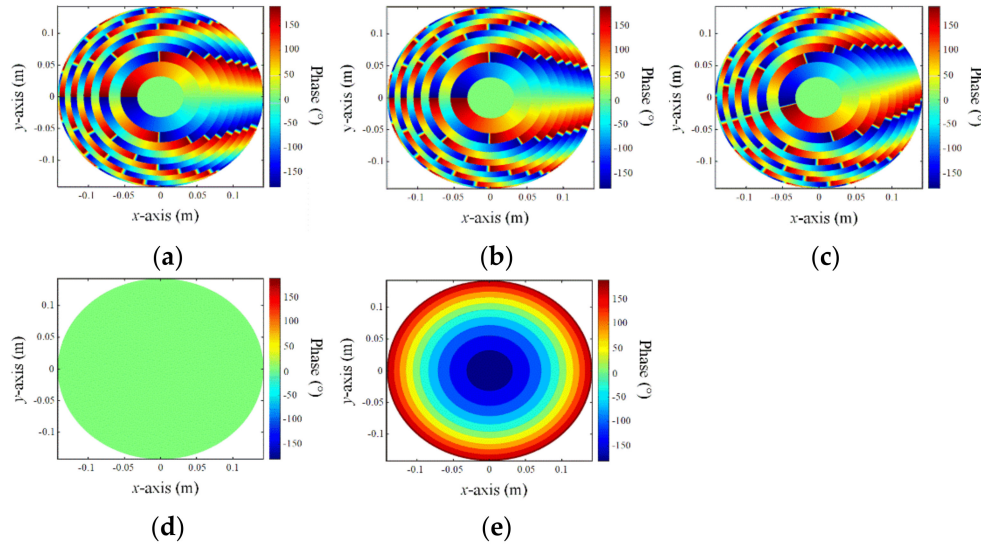


Figure 2. Transmitting phase distributions of Moiré lens: (a) T_1 ; (b) T_2 ($\theta_r = 0^\circ$); (c) T_2 ($\theta_r = 30^\circ$); (d) T_{12} ($\theta_r = 0^\circ$); and (e) T_{12} ($\theta_r = 30^\circ$).

Figure 2c shows the transmitting phase distributions when T_1 is fixed and T_2 is mechanically rotated by $\theta_r = 30^\circ$. T_2 can be re-derived considering the mechanical rotation as written in Equation (3).

$$T_2 = \begin{cases} \arg \left[\exp\{jk(ar^2)(\phi - \theta_r)\} \right] & \text{for } \theta_r \leq \phi < 360^\circ \\ \arg \left[\exp\{jk(ar^2)(\phi - \theta_r + 2\pi)\} \right] & \text{for } 0 \leq \phi < \theta_r \end{cases} \quad (3)$$

where θ_r is the mechanical rotation angle of T_2 changing from 0° to 360° . The transmitting phase distribution of T_{12} (phase after penetrating T_1 and T_2) can be calculated using the following equation:

$$T_{12} = T_1 + T_2 = \begin{cases} \arg \left[\exp\{jk(ar^2)\theta_r\} \right] & \text{for } \theta_r \leq \phi < 360^\circ \\ \arg \left[\exp\{jk(ar^2)(\theta_r - 2\pi)\} \right] & \text{for } 0 \leq \phi < \theta_r \end{cases} \quad (4)$$

The transmitting phase distributions of T_{12} according to the mechanical rotation of T_2 are shown in Figure 2d,e. When θ_r is set to 0° , the transmitting phase distribution becomes uniform due to the complex conjugate relationship between T_1 and T_2 (as shown in Figure 2d). On the other hand, when θ_r becomes 30° , the resulting transmitting phase distribution provides multiple circles, allowing adjustment of the focal point for electromagnetic power concentration (as shown in Figure 2e).

2.2. Design of Moiré MSL System

Figure 3 represents the geometry of the unit cell structure and the square patch antenna source, which are designed to operate at a frequency of 5.8 GHz. The unit cell has three RF-35 dielectric layers with a gap of h_2 ($\epsilon_r = 3.5$ and $\tan\delta = 0.0018$) as shown in Figure 3a. The unit cell has a periodic width of p and a height of h_1 . On the top and bottom dielectric layers, a square patch of length l_1 is printed, as shown in Figure 3b. In addition, a Jerusalem cross slot is etched on the middle dielectric layer as described in Figure 3c, and its shape is determined by w_1 , w_2 , and l_2 . Herein, this unit cell designed based on the previous study [25] can adjust the transmitting phase according to the Jerusalem slot length in the

middle layer because strong electromagnetic fields are confined in the region between the top and bottom patch layers, and the air gaps can increase the transmitting phase variations over 330° . To be specific, the top and bottom square patch layers can maintain high transmittance levels through the resonance characteristics, and the Jerusalem slot length dominantly affects the phase variation. The air gap between the layers can enhance the operating frequency bandwidths, which can increase the range of the phase variation. Figure 3d exhibits the square-shaped patch antenna printed on a RF-35 substrate ($\epsilon_r = 3.5$ and $\tan\delta = 0.0018$) with a height of h_3 to use as a source. The widths of the square patch and the ground are w_3 and g . Detailed parameters are listed in Table 1.

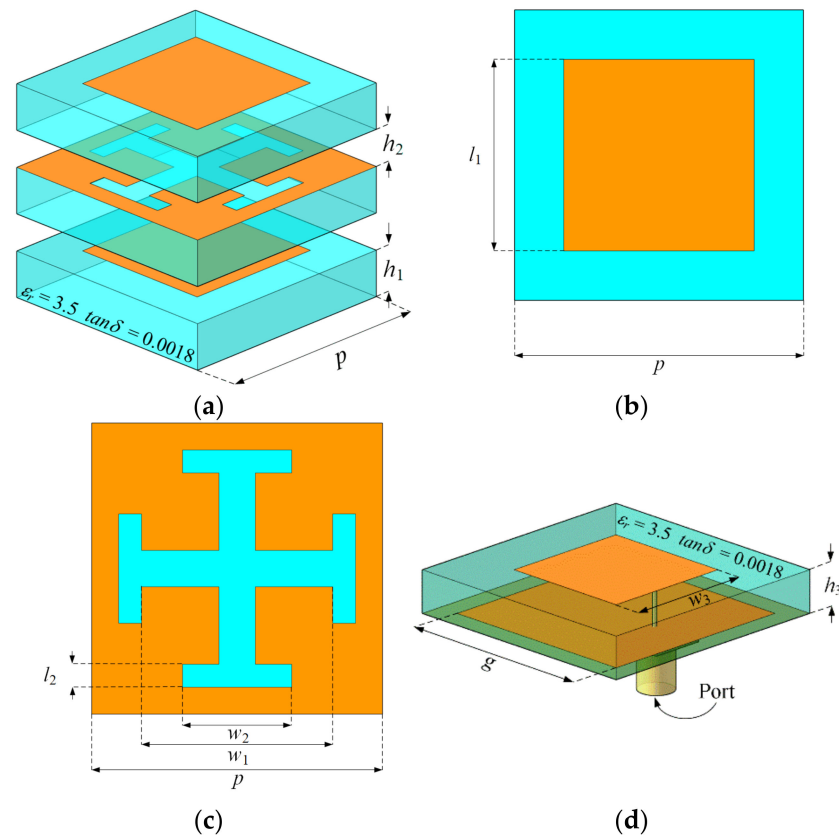


Figure 3. Geometry of the unit cell and the patch antenna: (a) isometric view of the unit cell; (b) top and bottom layers of the unit cell; (c) middle layer of the unit cell; and (d) patch antenna source.

Table 1. Design parameters for the unit cell and the patch antenna source.

Parameters	Values (mm)	Parameters	Values (mm)
p	51.7	l_2	0.4
h_1	1.56	w_1	7–18
h_2	1.56	w_2	1.9–12.9
h_3	1.56	w_3	12.8
l_1	7–18	g	40

Figure 4a shows the transmittance and phase variation by changing w_1 from 7 mm to 18 mm. The three-layered unit cell is electromagnetically coupled to each other, which can result the phase variation of up to 342° with the transmittance greater than -3 dB. In addition, the Jerusalem slot geometry can similarly achieve transmittance characteristics in accordance with the TE and TM modes due to the symmetric etched shapes; that is, the transmittance of the proposed MSL system can be less affected by the rotation of the second metasurface lens T_2 . Figure 4b presents the frequency responses of the transmittance and

phase characteristics ($w_1 = 13$ mm). The transmittance is greater than -3 dB in the operating frequency band from 4.8 GHz to 6.3 GHz, and the phase variation is achieved over 110° .

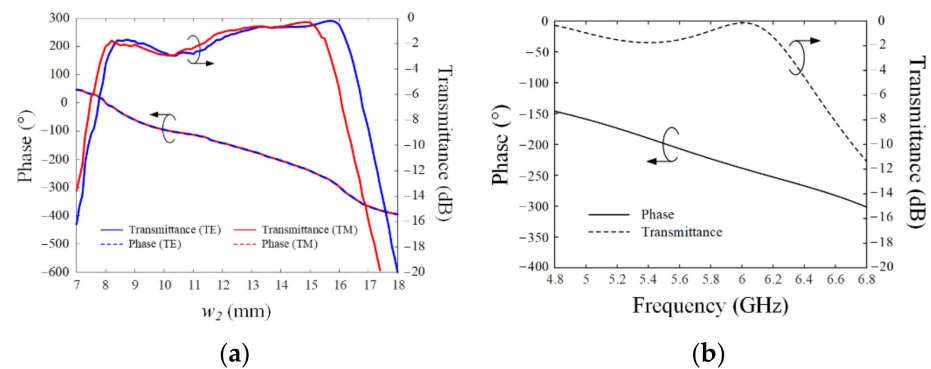


Figure 4. Transmittance and phase characteristics of the unit cell: (a) transmittance and phase characteristics according to for w_1 ; and (b) transmittance and phase characteristics by frequency.

To use the patch antenna as a source in the Moiré MSL system, it is essential to compensate phase distributions of the first MSL T_1 for the distance between the patch and T_1 . The near-field phase distribution of the stand-alone patch antenna needs to be obtained at the location on the bottom surface of T_1 considering the distance between the source and the MSL. The simple equation for the compensated phase distribution (T_1') is derived as follows:

$$T_1' = T_1 - P, \quad (5)$$

where P is the near-field phase distribution of the stand-alone patch antenna at the location on the bottom surface of the lens T_1 .

Figure 5a,b illustrate the calculated transmitting phase distributions of MSLs (T_1' and T_2) employing a total number of 354 unit-cells based on the Moiré lens theory. The MSLs for T_1' and T_2 are modeled using different unit cell structures, and each unit cell shape is specified to fit the transmitting phase distributions at each location. Figure 5c,d represent the final implementation models for the MSLs (T_1' and T_2) with a diameter of 28.5 cm (5.51λ). To confirm the theoretical phase distributions, each MSL is simulated to observe near-field transmitting phase distributions on the MSL's top surface, using the FEKO full EM simulation software tool, as shown in Figure 5e,f. In the simulation condition, an ideal incident wave is excited to each MSL, and the average phase deviations between the theoretical and simulated results for T_1' and T_2 are 19.4° and 15.9° , respectively.

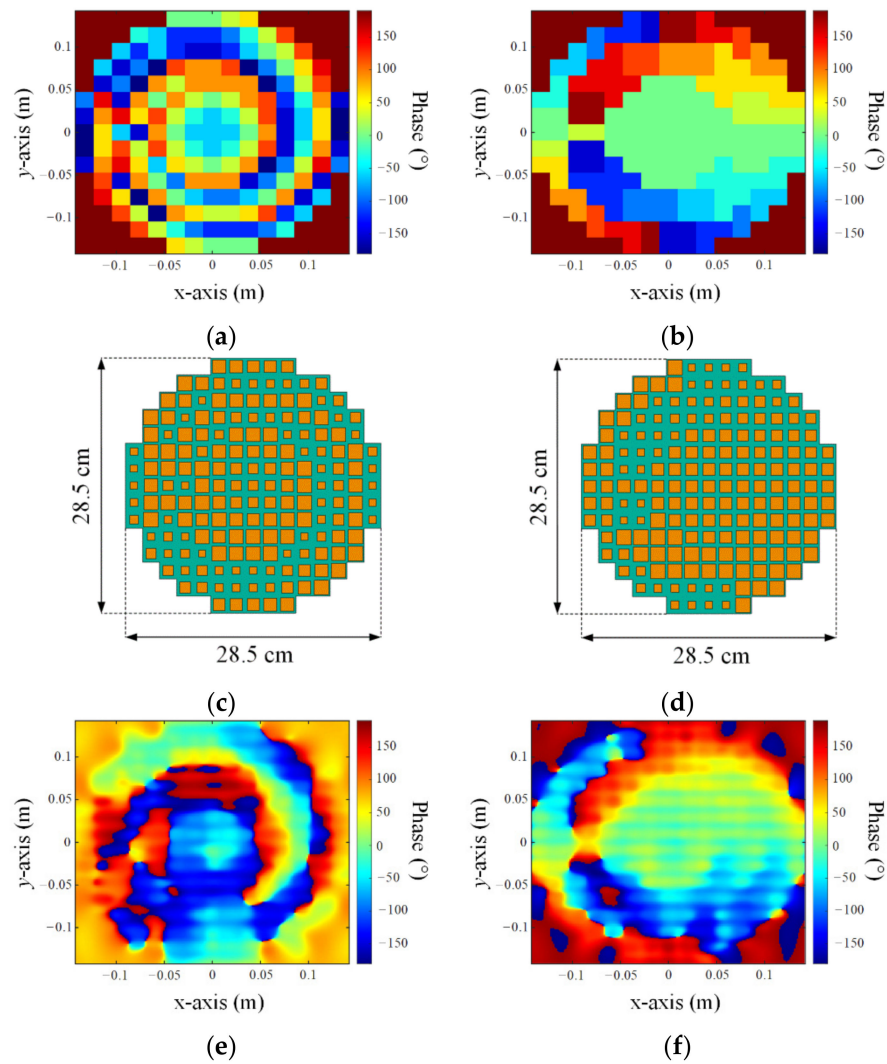


Figure 5. Transmitting phase distributions and geometry of the proposed MSLs: (a) theoretical transmitting phase distributions of T_1' ; (b) theoretical transmitting phase distributions of T_2 ; (c) simulation model of T_1' ; (d) simulation model of T_2 ; (e) simulated transmitting phase distributions of T_1' ; and (f) simulated transmitting phase distribution of T_2 .

3. Fabrication and Measurement

3.1. Moiré-Inspired MSL System Fabrication

Figure 6a–d show the fabricated MSLs (T_1' and T_2) using the unit cell structure (patch shape and Jerusalem cross slot shape). T_1' has identical upper and lower layers (Figure 6a) with a middle layer (Figure 6c). Similarly, T_2 has identical upper and lower layers (Figure 6b) with a middle layer (Figure 6d). The square patch antenna (Figure 6e) is printed on the center of the substrate that has the same diameter as the MSLs. On the opposite side, it has a ground, and the SMA connector is used as a feeder. All layers have small circular holes to joint to each other using plastic and metallic volts and nuts. Figure 6f presents the proposed Moiré-inspired MSL system, fully assembled with a Styrofoam zig to hold the layers.

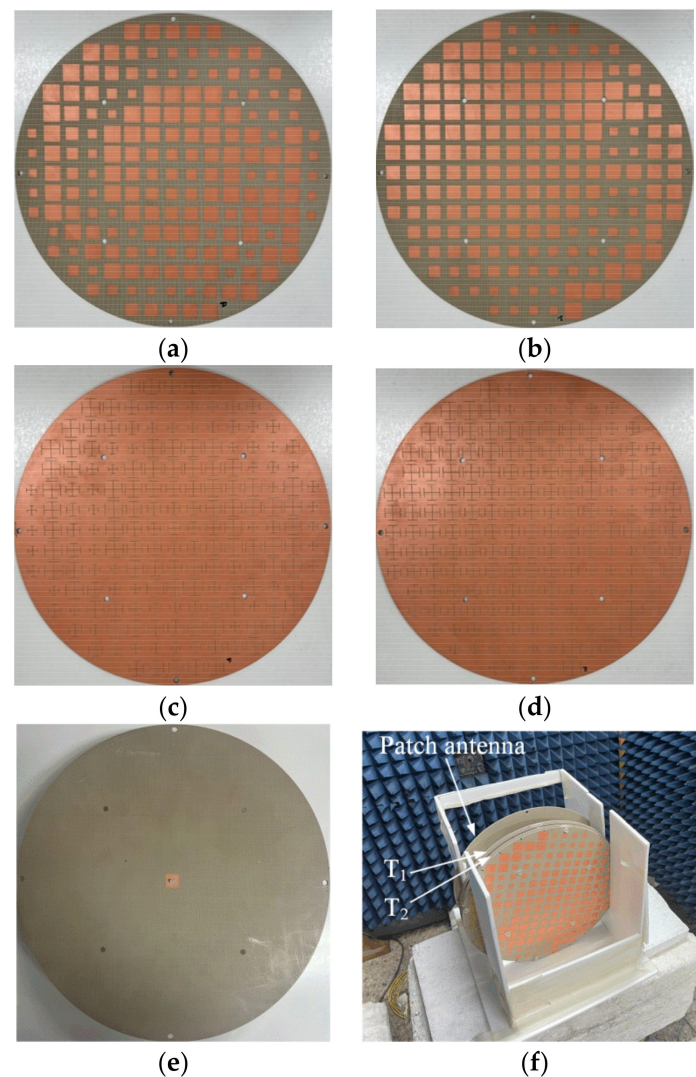


Figure 6. Photographs of the fabricated Moiré-inspired MSL system: (a) upper and lower layers of T_1' ; (b) upper and lower layers of T_2 ; (c) middle layer of T_1' ; (d) middle layer of T_2 ; (e) patch antenna layer; and (f) fully assembled MSL system.

To verify that the focal point of electromagnetic power can be adjustable in the near field region using the proposed Moiré-inspired MSL system, T_1' and T_2 are arranged to have an interval of 5 mm along the z -axis. The patch antenna is located at the distance of 50 mm from T_1' to excite the field to the MSLs. To measure the electromagnetic power in the near-field region, the HP8753D vector network analyzer and a horn antenna (BBHA 9120 D) are used in the measurement setup, as shown in Figure 7. The near-field is measured (from 12 cm to 122 cm at intervals of 10 cm) according to the rotation angles from $\theta_r = 0^\circ$ to 90° with an angle interval of 15° . In addition, reflection coefficients of the proposed MSL system are measured according to the rotation angles.

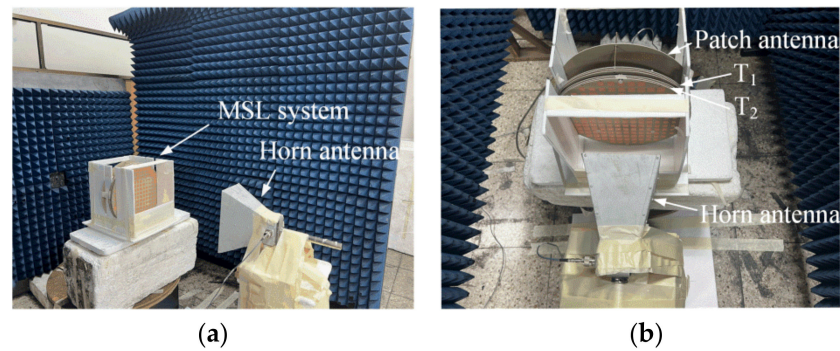


Figure 7. Photographs of measurement setup for the proposed Moiré-inspired MSL system: (a) isometric view; and (b) top view.

3.2. Moiré-Inspired MSL System Measurement

Figure 8 shows measured and simulated reflection coefficients of the proposed MSL system according to the rotation angle θ_r . The measured reflection coefficients are under -10 dB at 5.8 GHz for all rotation angles. Figure 9 represents the measured and simulated normalized near-E-field distributions along the z -axis according to the rotation angle. The simulated and measured results show that the near-E-field gradually degrades by $1/(\text{squared distance between the horn and the MSL})$ in the Fresnel near-field region. We can also observe that the focal point of the near-field beam can be changed by rotating the angle of T_2 from $\theta_r = 0^\circ$ to 90° . For example, if we draw a specific normalized E-field level line (0.2 in this case), then the focal length of the measurements is adjusted from a minimum of 38 cm to a maximum of 110 cm, and that of the simulation is changed from 42 cm to 62 cm, as shown in Figure 10. The measured and simulated results exhibit similar trends for adjustment of the focal point until the rotation angle of 60° ; however, some deviations between the simulation and measurement in the angle range from 75° to 90° are observed due to the tolerance errors in the fabrication process. Note that the focal point in the long-range region can be more obviously adjusted having a linear characteristic if the MSL size becomes enlarged over 10λ [26]. Figure 11 shows near-E-field distributions in the zy -plane according to the rotation angles. The results clearly show that the focal point of electromagnetic power is changed according to the rotation angle. Furthermore, in terms of the wireless electromagnetic energy transfer, we also analyze the transmission efficiency (η_{MSL}) of the MSLs and the wireless power transfer efficiency (η_{WPT}) at the focal length according to the rotation angle of T_2 . η_{MSL} and η_{WPT} are calculated based on the equations as follows [4,27]:

$$\eta_{MSL} = \frac{\iint |E_{out}(x, y)|^2 ds}{\iint |E_{in}(x, y)|^2 ds}, \quad (6)$$

$$\eta_{WPT} = \frac{P_r(z_0)}{P_t}, \quad (7)$$

where E_{out} and E_{in} are the near-E-fields on the top and bottom plane of the MSLs, and P_t and $P_r(z_0)$ are the transmitting power and the receiving power at the focal length of z_0 . Figure 12 illustrates the transmission efficiency and the wireless power transfer efficiency according to the rotation angle θ_r . η_{MSL} can maintain over 24.5% according to the rotation angle, and η_{WPT} has a maximum level of 40.4% at the rotation angle of 45° .

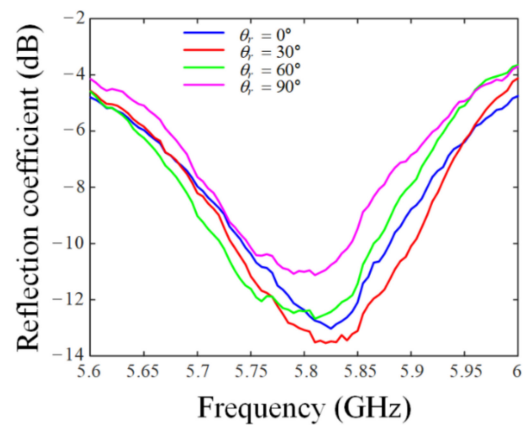


Figure 8. Reflection coefficient of the Moiré-inspired MSL system according to the rotation angle.

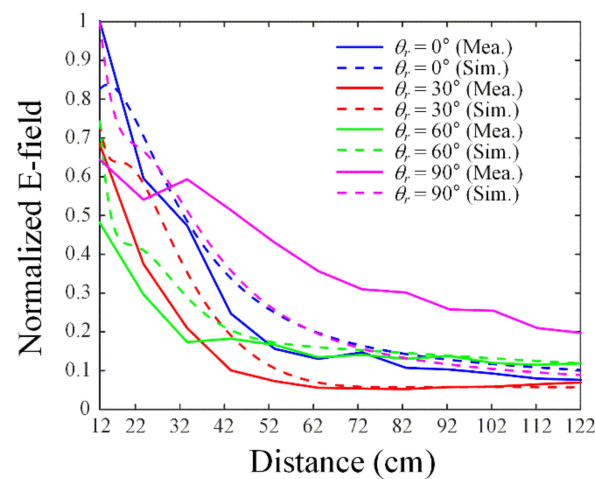


Figure 9. Measured and simulated normalized near-E-field distributions along the z-axis according to the rotation angle.

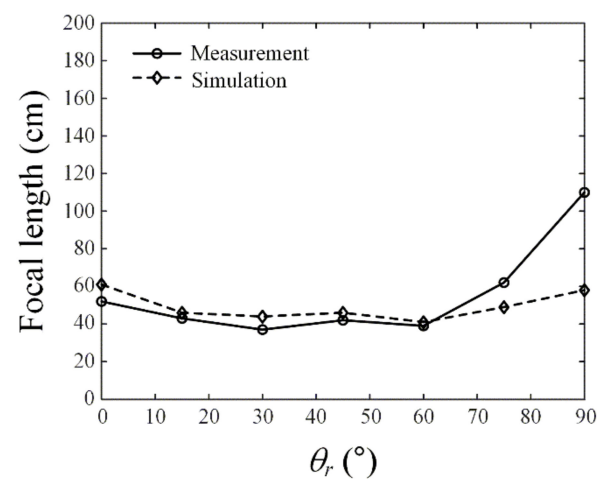


Figure 10. Measured and simulated focal length according to the rotation angle.

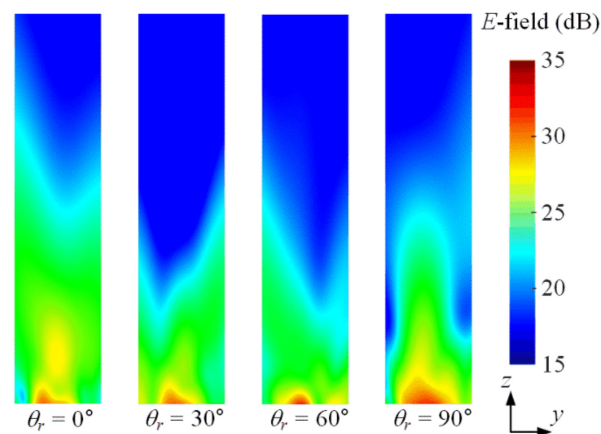


Figure 11. E-field distributions according to θ_r in the zy -plane.

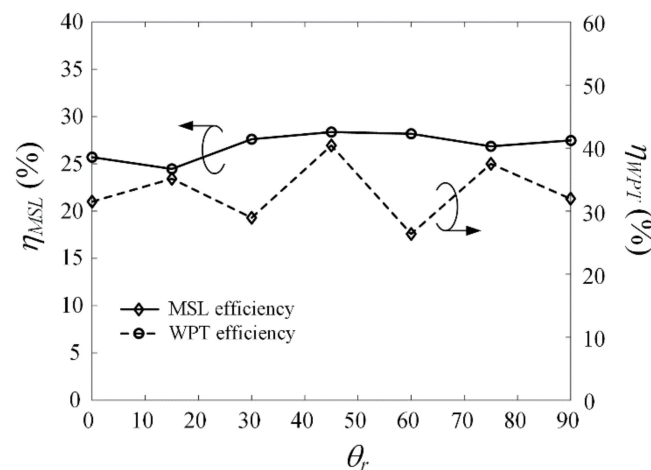


Figure 12. Simulated transmission efficiency and wireless power transfer efficiency according to the rotation angle.

The results confirm that the proposed Moiré-inspired MSL system is capable of changing the focal point of electromagnetic power in the near-field region simply by rotating the MSL.

4. Conclusions

In this paper, we proposed a Moiré-inspired MSL system for focusing electromagnetic power in the Fresnel near-field region. The proposed MSL system consisted of two lenses and a square patch antenna source. The two MSLs were modeled based on the transmitting phase distributions of Moiré lens theory using the three-layered unit cell structure, which included two square patches and one Jerusalem cross slot shape patch. The phase and transmittance variations of the unit cell were over 330° and -3 dB according to the unit cell structure. The square patch antenna source was also designed to excite the field to the MSLs. To confirm the feasibility, the proposed MSL system was fabricated, and its near-field and matching characteristics were measured. The measured reflection coefficients were under -10 dB at 5.8 GHz for all rotation angles. The focal length of the measurements was adjusted from a minimum of 38 cm to a maximum of 110 cm when changing the rotation angle of the second MSL. The results demonstrated that the proposed Moiré-inspired MSL system was capable of adjusting the beam focusing of the electromagnetic power in the Fresnel near-field region. In future work, the MSL system might be employed for the practical WPT applications to focus electromagnetic power at various locations in the near-field region, and its performance can be enhanced by increasing the fabrication tolerances and the total dimension of the MSL.

Author Contributions: Conceptualization, T.-H.L., H.K. and H.C.; methodology, T.-H.L.; software, T.-H.L. and H.K.; validation, T.-H.L., H.K., C.S. and H.C.; formal analysis, T.-H.L.; investigation, T.-H.L.; resources, H.C.; data curation, H.K.; writing—original draft preparation, T.-H.L., H.K.; writing—review and editing, T.-H.L., H.K. and H.C.; visualization, T.-H.L. and H.K.; supervision, H.C.; project administration, C.S. and H.C.; funding acquisition, C.S. and H.C. All authors have read and agreed to the published version of the manuscript.

Funding: This research was funded by the Basic Science Research Program through the National Research Foundation of Korea (NRF) funded by the Ministry of Education (no. NRF-2017R1A5A1015596), and the NRF grant funded by the Korea government (no. 2015R1A6A1A03031833).

Institutional Review Board Statement: Not applicable.

Informed Consent Statement: Not applicable.

Data Availability Statement: Not applicable.

Conflicts of Interest: The authors declare no conflict of interest.

References

1. Siragusa, R.; Lemaire-Auger, P.; Tedjini, S. Tunable near-field focused circular phase-array antenna for 5.8-GHz RFID applications. *IEEE Antennas Wirel. Propag. Lett.* **2011**, *10*, 33–36. [[CrossRef](#)]
2. Gowda, V.R.; Yurduseven, O.; Lipworth, G.; Zupan, T.; Reynolds, M.S.; Smith, D.R. Wireless power transfer in the radiative near field. *IEEE Antennas Wirel. Propag. Lett.* **2016**, *15*, 1865–1868. [[CrossRef](#)]
3. Kim, G.; Lee, B. Design of wireless power and information transfer systems considering figure of merit for information. *J. Electromagn. Eng. Sci.* **2020**, *20*, 241–247. [[CrossRef](#)]
4. Kang, E.; Hur, J.; Seo, C.; Lee, H.; Choo, H. High aperture efficiency array antenna for wireless power transfer applications. *Energies* **2020**, *13*, 2241. [[CrossRef](#)]
5. Ahmad, Z.; Wang, Z.; Jaffri, Z.U.A.; Bao, S. Accurate theoretical models for frequency diverse array based wireless power transmission. *Energies* **2022**, *15*, 1588. [[CrossRef](#)]
6. Shan, L.; Geyi, W. Optimal design of focused antenna arrays. *IEEE Trans. Antennas Propag.* **2014**, *62*, 5565–5571. [[CrossRef](#)]
7. Liu, Y.; Cheng, Q.; Khan, A.N.; Giddens, H.; Torrico, M.M.; Hao, Y. Low-profile beam steerable patch array with SIW feeding network. *IEEE Access* **2020**, *8*, 164178. [[CrossRef](#)]
8. Li, M.; Chang, K. Novel low-cost beam-steering techniques using microstrip patch antenna arrays fed by dielectric image lines. *IEEE Trans. Antennas Propag.* **1999**, *47*, 453–457. [[CrossRef](#)]
9. Hansen, R.C. Focal region characteristics of focused array antennas. *IEEE Trans. Antennas Propag.* **1985**, *33*, 1328–1337. [[CrossRef](#)]
10. Nikfalazar, M.; Kohler, C.; Wiens, A.; Mehmood, A.; Sohrabi, M.; Maune, H.; Binder, J.R.; Jakoby, R. Beam steering phased array antenna with fully printed phase shifters based on low-temperature sintered BST-composite thick films. *IEEE Microw. Wirel. Compon. Lett.* **2016**, *26*, 70–73. [[CrossRef](#)]
11. Rana, B.; Lee, I.-G.; Hong, I.-P. Experimental characterization of 2×2 electronically reconfigurable 1bit unit cells for a beamforming transmitarray at x band. *J. Electromagn. Eng. Sci.* **2021**, *21*, 153–160. [[CrossRef](#)]
12. Hu, J.; Li, Y.; Zhang, Z. A novel reconfigurable miniaturized phase shifter for 2-D beam steering 2-bit array applications. *IEEE Microw. Wirel. Compon. Lett.* **2021**, *31*, 381–384. [[CrossRef](#)]
13. Sheikh, S.I.M.; Gibson, A.A.P.; Basorrah, M.; Alhulwah, G.; Alanizi, K.; Alfarsi, M.; Zafar, J. Analog/digital ferrite phase shifter for phased array antennas. *IEEE Antennas Wirel. Propag. Lett.* **2010**, *9*, 319–321. [[CrossRef](#)]
14. Lim, T.-H.; Seo, C.; Choo, H. Design of a metasurface lens to adjust the focal length for near-field beam focusing. *J. Korean Inst. Electromagn. Eng. Sci.* **2021**, *32*, 610–615. [[CrossRef](#)]
15. Xue, C.; Lou, Q.; Chen, Z.N. Broadband double-layered Huygens' metasurface lens antenna for 5G millimeter-wave systems. *IEEE Trans. Antennas Propag.* **2020**, *68*, 1468–1476. [[CrossRef](#)]
16. Pfeiffer, C.; Grbic, A. Planar lens antennas of subwavelength thickness: Collimating leaky-waves with metasurfaces. *IEEE Trans. Antennas Propag.* **2015**, *63*, 3248–3253. [[CrossRef](#)]
17. Xu, R.; Chen, Z.N. A compact beamsteering metasurface lens array antenna with low-cost phased array. *IEEE Trans. Antennas Propag.* **2021**, *69*, 1992–2002. [[CrossRef](#)]
18. Altair. FEKO. Available online: www.altair.com (accessed on 29 March 2022).
19. Liu, Z.; Du, Z.; Hu, B.; Liu, W.; Liu, J.; Wang, Y. Wide-angle Moiré metalens with continuous zooming. *J. Opt. Soc. Am. B* **2019**, *36*, 2810–2816. [[CrossRef](#)]
20. Bernet, S.; Harm, W.; Ritsch-Marte, M. Demonstration of focus-tunable diffractive Moiré-lenses. *Opt. Express* **2013**, *21*, 6955–6966. [[CrossRef](#)] [[PubMed](#)]
21. Lee, J.G. Tutorial: Reconfigurable transmitarray antenna using metasurface. *J. Korean Inst. Electromagn. Eng. Sci.* **2020**, *31*, 663–676. [[CrossRef](#)]
22. Oster, G.; Nishijima, Y. Moiré patterns. *Sci. Am.* **1963**, *208*, 55–63. [[CrossRef](#)]

23. Oster, G.; Wasserman, M.; Zwerling, C. Theoretical interpretation of Moiré patterns. *J. Opt. Soc. Am.* **1964**, *54*, 169–175. [[CrossRef](#)]
24. Bernet, S.; Ritsch-Marte, M. Adjustable refractive power from diffractive moiré elements. *Appl. Opt.* **2008**, *47*, 3722–3730. [[CrossRef](#)]
25. Li, M.-Y.; Ban, Y.-L.; Yan, F.-Q. Wideband low-profile Ku-band transmitarray antenna. *IEEE Access* **2020**, *9*, 6683–6688. [[CrossRef](#)]
26. Iwami, K.; Ogawa, C.; Nagase, T.; Ikezawa, S. Demonstration of focal length tuning by rotational varifocal moiré metalens in an ir-A wavelength. *Opt. Express* **2020**, *28*, 35602–35614. [[CrossRef](#)] [[PubMed](#)]
27. Balanis, C.A. *Antenna Theory: Analysis and Design*, 4th ed.; Wiley: Hoboken, NJ, USA, 2016.